Sensors and Materials, Vol. 38, No. 5 (2026) 2789–2798
MYU Tokyo

S & M 4469

Supercritical CO_2-assisted Deposition of TiO_2 Nanoparticles for High-performance Nonenzymatic Glucose Sensors

Yu-Chun Huang* and Cong-Yi Sun

Department of Electrical Engineering, Southern Taiwan University of Science and Technology, Tainan 71005, Taiwan

(Received August 21, 2025; accepted May 14, 2026)

Keywords: nonenzymatic glucose sensor, rutile/anatase TiO_2, supercritical CO_2 deposition, hydrothermal synthesis, electrochemical detection

In this study, a nonenzymatic glucose sensor was fabricated through a three-step process on fluorine-doped tin oxide (FTO) conductive glass. First, rutile-phase TiO_2 nanorods were synthesized via a hydrothermal method to form a stable sensing structure. Subsequently, anatase-phase TiO_2 nanoparticles were deposited using a supercritical carbon dioxide ($scCO_2$)-assisted static deposition technique, which increased surface roughness and the number of electroactive sites. Finally, Au nanoparticles were sputtered onto the TiO_2 heterostructure to enhance conductivity and electron transfer efficiency. In this paper, we present a feasible approach for developing high-performance nonenzymatic glucose sensors with potential applications in wearable healthcare devices, point-of-care diagnostics, and biochemical sensing systems.

1. Introduction

Glucose is the most important metabolic substrate in the human body, serving as a primary energy source for the brain and red blood cells and participating in essential processes such as glycoprotein synthesis and glycogen storage.[1,2] Accurate glucose monitoring is thus of great clinical significance for the early diagnosis of diabetes, treatment monitoring, and complication prevention.[3–5]

Electrochemical glucose sensors are broadly divided into enzymatic and nonenzymatic types. Enzymatic sensors rely on glucose oxidase (GOx) or glucose dehydrogenase (GDH) to generate measurable electrochemical signals, offering high selectivity and sensitivity within the physiological range.[6] However, their practical application is hindered by high enzyme cost, poor stability against temperature and pH fluctuations, and the complexity of enzyme immobilization. These limitations result in reduced durability and increased manufacturing difficulty.

Nonenzymatic glucose sensors, in contrast, utilize transition metals (Ni, Cu, and Co), their oxides, alloys, or carbon-based materials as catalysts to directly oxidize glucose without using

*Corresponding author: e-mail: ych0321@stust.edu.tw
https://doi.org/10.18494/SAM5913

ISSN 0914-4935
https://myukk.org/

enzymes. Such materials are inexpensive, widely available, and chemically stable, providing enhanced durability under varied environmental conditions.[7–9] Fabrication methods such as electrochemical deposition, hydrothermal synthesis, and chemical vapor deposition enable the preparation of high-surface-area nanostructures under relatively mild conditions, making nonenzymatic sensors attractive for scalable production.

Among candidate materials, TiO_2 has drawn considerable attention owing to its chemical stability, biocompatibility, and tunable crystal phases. The anatase phase exhibits high catalytic activity, while the rutile phase provides structural stability. Combining these phases with nanostructure engineering and noble metal modification offers opportunities to enhance sensitivity and long-term reliability.[10,11] Recent biochemical sensing systems have increasingly emphasized miniaturization, portability, and integration with wearable or implantable platforms such as BioMEMS, lab-on-chip devices, and self-powered sensors. However, many existing systems still rely on enzyme-based electrodes with limited long-term stability. Therefore, developing stable nonenzymatic sensing materials remains highly important for future biochemical sensing systems.

In this work, we propose a rutile-phase TiO_2 platform integrated with anatase nanostructures, enhanced through two modification strategies: the supercritical CO_2-assisted deposition of TiO_2 nanoparticles and sputtered gold nanoparticles. This hybrid design aims to achieve high sensitivity and superior long-term stability.

2. Experimental Methods

In this study, a three-step fabrication process was employed to develop the glucose sensor. Figure 1 illustrates the schematic structure of the stacked sensor, while Fig. 2 presents the overall fabrication workflow and measurement procedures.

2.1 Materials

Fluorine-doped tin oxide (FTO) conductive glass substrates (1 × 1.5 cm^2, purchased from Ruilong Optoelectronics, Taiwan) were used as transparent conducting electrodes. Titanium(IV)

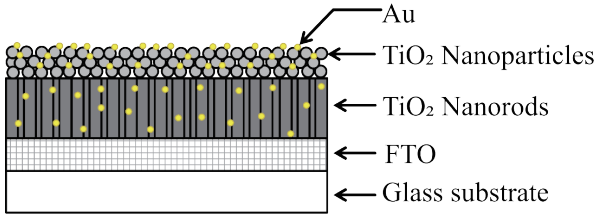

Fig. 1. (Color online) Schematic illustration of the stacked glucose sensor structure.

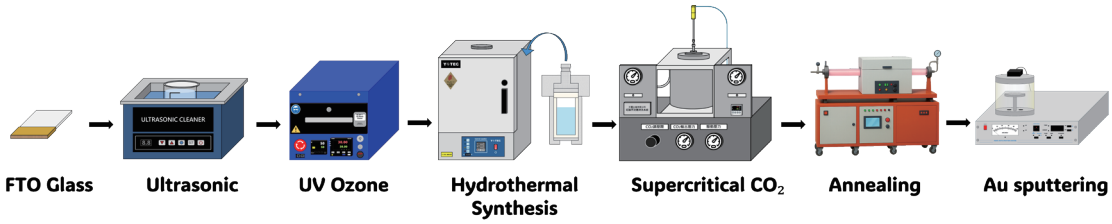

Fig. 2. (Color online) Schematic illustration of the fabrication process flow.

butoxide $Ti(OBu)_4$ (TBOT, ≥97%) was obtained from Alfa Aesar (CAS: 5593-70-4) and used as the titanium precursor without further purification. Hydrochloric acid (HCl, 36 wt%, CAS: 7647-01-0) was purchased from a local supplier and used as received.

2.2 Fabrication process

2.2.1 Pretreatment and hydrothermal synthesis

The FTO glass substrates were first pretreated by masking the electrode region with heat-resistant tape to prevent the contamination of nonreactive areas. The substrates were sequentially cleaned by ultrasonication in acetone, isopropanol, and deionized (DI) water, followed by UV-ozone treatment to ensure a clean surface favorable for subsequent film deposition. The hydrothermal precursor solution was prepared by mixing concentrated HCl (36 wt%) with DI water, followed by the dropwise addition of TBOT using a micropipette. Since concentrated HCl releases heat upon dilution, precautions were taken to avoid local overheating, splashing, or boiling. Three precursor solutions with different compositions, namely, 30:30:0.9, 30:30:2.0, and 30:30:2.5 mL (HCl:DI water:TBOT), were prepared. Hydrothermal synthesis was then conducted by immersing the pretreated FTO substrates into the solution contained in a Teflon-lined cup, which was sealed in a stainless-steel autoclave and heated at 160 ℃ for 4 h to form TiO_2 films.

2.2.2 $scCO_2$-assisted Deposition and Post-treatment

TiO_2 nanoparticles were further deposited onto the TiO_2 films using the supercritical carbon dioxide ($scCO_2$) technique. The crystalline phase of TiO_2 depends strongly on the preparation and post-treatment conditions. It was previously reported that the as-prepared TiO_2 is typically amorphous, while anatase is preferentially formed after thermal treatment or extended reaction.[12] At higher annealing temperatures (≈750 ℃), anatase tends to transform into rutile. In this study, thermal annealing was carried out in a tube furnace with a final annealing temperature of 450 ℃, using a stepwise heating program of 80 ℃ for 0.5 h, 150 ℃ for 1 h, 300 ℃ for 1 h, and 450 ℃ for 1 h, followed by natural cooling. Finally, gold nanoparticles were sputtered onto the TiO_2 films at a discharge current of 30 mA and a working pressure of 0.05 mbar to ensure a stable deposition rate and uniform thin-film formation.

2.3 Fabrication of TiO_2 films via $scCO_2$ static deposition

$scCO_2$ deposition is a green fabrication technique that operates above critical point (31.1 ℃ and 7.38 MPa), where CO_2 simultaneously exhibits the density of a liquid and the diffusivity of a gas. This unique property has led to its wide application in the synthesis of nanomaterials and functional thin films. The advantages of $scCO_2$ include low toxicity, low surface tension, high diffusivity, and tunable solvating power, which allow for the synthesis of high-quality TiO_2 materials under mild conditions.

The principle of supercritical fluid-assisted static deposition (SFASD) is based on the high diffusivity and carrier capacity of $scCO_2$. Under supercritical conditions, CO_2 exhibits a gas-like

diffusion coefficient (~10^{-4} cm^2/s) and a liquid-like density, enabling it to penetrate porous substrates and transport precursor molecules. Upon reaching the substrate surface or pores, the precursor undergoes hydrolysis and condensation reactions, resulting in the formation of a uniform TiO_2 deposition layer. The mass transport during this process can be described by Fick's second law:

$$\partial C/\partial t = D\nabla^2 C, \tag{1}$$

where C is the solute concentration, t is the time, D is the diffusion coefficient, and $\nabla^2 C$ represents the Laplacian operator of concentration.[13]

In this work, TiO_2 thin films were fabricated on FTO conducting glass substrates by $scCO_2$ static deposition. Prior to deposition, the reaction chamber was preheated to 60 °C and maintained for 2 h to ensure thermal equilibrium. A precursor solution was prepared by dissolving 1.36 mL of TBOT in 10 mL of IPA, which was then placed in a 20 mL scintillation vial. The FTO substrates were ultrasonically cleaned sequentially with acetone, IPA, and DI water, and positioned on a glass Petri dish with the conductive side facing upward. Both the scintillation vial and the substrate were then loaded into a high-pressure reactor. After sealing the system, CO_2 was introduced and the pressure was adjusted to 1500–3500 psi (≈10.3–24.1 MPa) to achieve supercritical conditions, as illustrated in Fig. 3.

3. Results and Discussion

In this section, the structural, morphological, compositional, and electrochemical characteristics of the fabricated TiO_2-based glucose sensors are systematically analyzed and discussed. A combination of spectroscopic, microscopic, and electrochemical techniques was employed to evaluate the material properties and sensing performance. Raman spectroscopy was utilized to investigate the crystalline phases of TiO_2 films and to assess the effect of the supercritical CO_2 deposition process on structural stability. The surface morphology and particle distribution were examined by field-emission scanning electron microscopy (FE-SEM), while energy-dispersive X-ray spectroscopy (EDX) provided complementary information on elemental

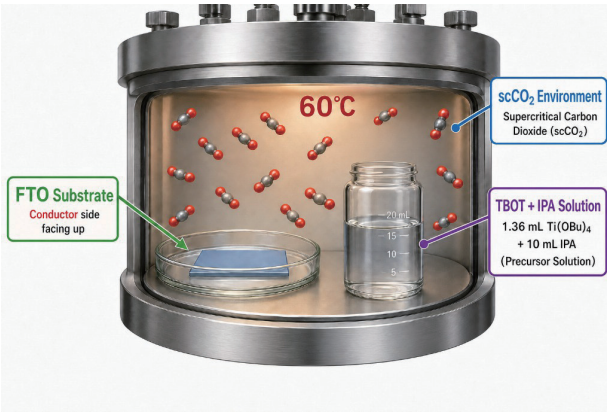

Fig. 3. (Color online) Schematic illustration of the $scCO_2$-assisted static deposition process for TiO_2 thin films on FTO substrates.

composition and nanoparticle dispersion. Electrochemical analyses, including cyclic voltammetry (CV) and sensitivity evaluation, were performed to elucidate the device's glucose oxidation behavior, assess its sensing performance, and benchmark its response against previously reported sensors. The combined results provide a comprehensive understanding of the relationship between film structure, morphology, and electrochemical properties, thereby highlighting the advantages of employing $scCO_2$-assisted deposition in biosensor fabrication.

3.1 FE-SEM

The effect of precursor concentration on the morphology of TiO_2 nanostructures was systematically investigated by FE-SEM. Under fixed acidic conditions (HCl:DI water = 30:30 mL, pH < 0.1), the hydrolysis ratio (H_2O/Ti) decreased from 1151 to 518 to 414 as the TBOT content increased from 0.9 to 2.0 to 2.5 mL, respectively. This variation significantly affected the nucleation and growth mechanism of TiO_2, thereby altering the resulting morphology.

As shown in Fig. 4(a), (H_2O/Ti = 1151) exhibited well-aligned nanorod arrays with an average diameter of 168.4 nm, while in Figs. 4(b) and 4(c), (H_2O/Ti = 518 and 414) presented thinner nanorods with average diameters of 78.4 and 63.9 nm, respectively. However, only sample 1 demonstrated a defect-free surface when observed at 30,000× magnification, whereas samples 2 and 3 revealed partial voids where the FTO substrate remained exposed, indicating incomplete nanorod coverage.

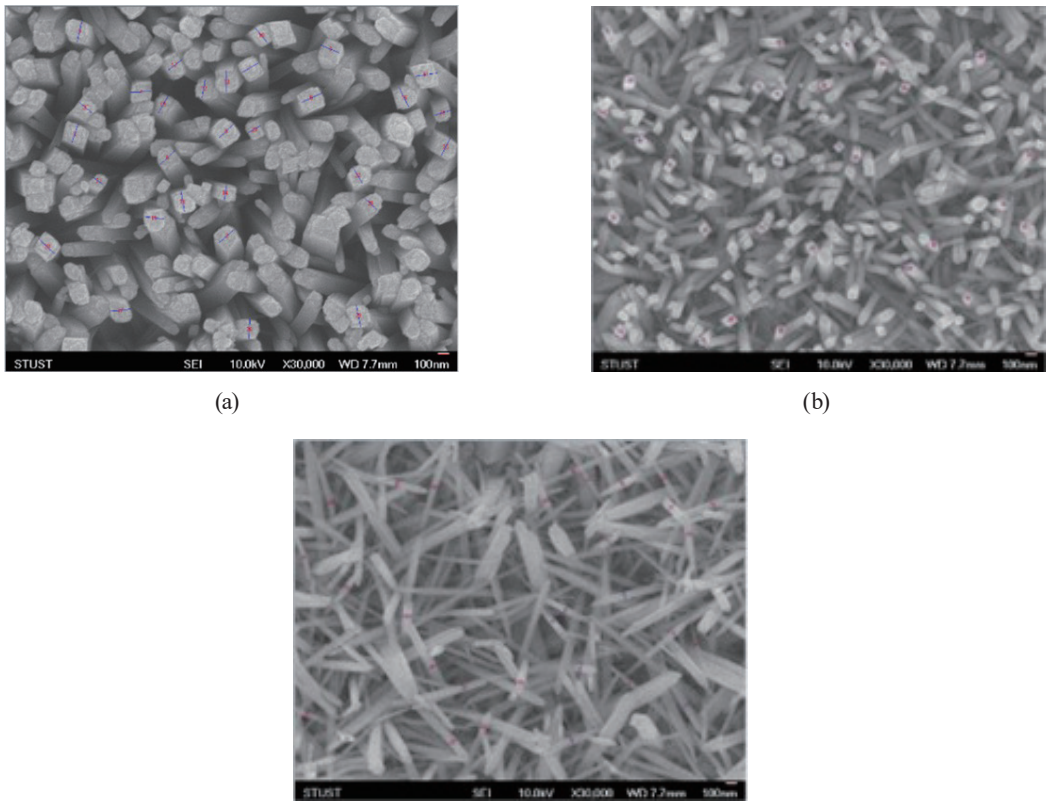

(a) (b)

(c)

Fig. 4. (Color online) FE-SEM images of TiO_2 nanostructures with different TBOT contents: (a) 0.9 mL, (b) 2.0 mL, and (c) 2.5 mL. Increasing the precursor concentration reduces the H_2O/Ti ratio and significantly alters the morphology.

Considering subsequent processing durability, sample 1 (30:30:0.9) was selected as the baseline structure for further sensor fabrication. The thicker nanorods provide a larger cross-sectional area, reducing the likelihood of bending or fracture under mechanical stress, friction, or ultrasonic cleaning. This enhanced structural robustness is particularly advantageous for applications requiring repeated usage and cleaning, such as electrochemical sensors or catalyst supports, where mechanical stability is a critical performance factor.

3.2 Raman spectroscopy

To further confirm the crystalline phase of the hydrothermally synthesized TiO_2 nanostructures, Raman spectroscopy was performed on sample 1 under different reaction durations (2 and 4 h). Figure 5 shows the corresponding Raman spectra. Both spectra exhibit characteristic peaks at 447 and 612 cm^{-1}, along with a distinct band at ~235 cm^{-1}. These features are well-established fingerprint signatures of the rutile-phase TiO_2. Specifically, the peak at 447 cm^{-1} corresponds to the Eg mode, while the band at 612 cm^{-1} is attributed to the A1g mode. The additional peak at ~235 cm^{-1} is associated with second-order phonon scattering, which has been widely reported as a hallmark of rutile TiO_2 in the literature.

Importantly, the Raman intensity of the 4 h sample is significantly higher than that of the 2 h counterpart, suggesting improved crystallinity and more complete phase development with extended reaction time. This result indicates that prolonging the hydrothermal duration from 2 to 4 h promotes a better-defined rutile crystal structure, which is expected to enhance the stability and performance of the TiO_2-based sensing electrode.

Since the electrochemical activity of TiO_2 is strongly correlated with its crystal phase and degree of crystallinity, the confirmation of a well-developed rutile structure provides a crucial foundation for interpreting the subsequent electrochemical measurements and sensitivity analysis.

3.2.1 EDX

To further verify the elemental composition of the prepared electrodes, EDX analysis was conducted on sample 1 after completing the three steps of the fabrication process, namely, (1)

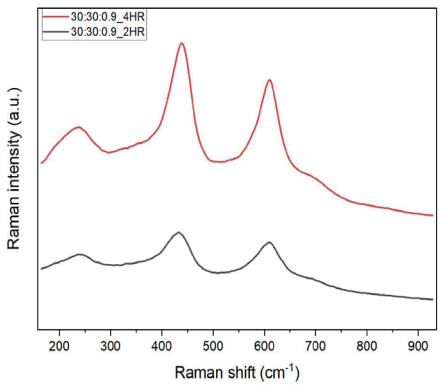

Fig. 5. (Color online) Raman spectra of TiO_2 films synthesized at different hydrothermal reaction times.

hydrothermal synthesis, (2) $scCO_2$-assisted TiO_2 deposition, and (3) Au sputtering. The results are summarized in Table 1.

The EDX spectrum confirms the presence of the expected elements O, Ti, and Au, along with Sn originating from the underlying FTO glass substrate. Since FTO is primarily composed of SnO_2 with a small amount of fluorine doping to enhance conductivity, the detection of Sn is reasonable and consistent with the electrode structure. The measured atomic percentages are 76.88% for O, 16.99% for Ti, 5.62% for Sn, and 0.51% for Au, yielding a total weight concentration of 17.33 wt%.

These findings confirm that the three-step fabrication process successfully incorporated the intended components without introducing undesired impurities. In particular, the detection of Au validates the effectiveness of the sputtering process, which plays a crucial role in improving the electrode's surface conductivity and enhancing electrochemical activity in subsequent measurements.

3.3 Electrochemical measurements

Electrochemical measurements were performed using a CH Instruments CHI6116F electrochemical workstation in a standard three-electrode configuration. The working electrode was the TiO_2-based sensing electrode fabricated in this study, the reference electrode was Ag/AgCl, and a platinum wire was used as the counter electrode. The supporting electrolyte was 0.1 M NaOH solution.

3.3.1 CV

CV was conducted to evaluate the electrochemical performance of the glucose sensors. Measurements were performed at a scan rate of 0.1 V/s in glucose solutions of 20 mM. In CV, the electrode potential is cyclically swept within a defined range, and the resulting current response is recorded to probe redox reaction mechanisms and electrode kinetics. Prior to formal measurements, a wide-potential-range scan from −1.0 to +1.0 V was conducted to activate the electrode surface. Subsequent measurements were carried out within a narrower range (−0.4 to +0.4 V) to capture glucose oxidation responses.

Figure 6 presents the CV responses of three electrode configurations in 20 mM glucose solution: (i) hydrothermally synthesized TiO_2 with $SCFTiO_2$ coating and Au deposition (HT+SCF+A+Au, red curve), (ii) hydrothermal synthesis with $SCFTiO_2$ coating but without Au deposition (HT+SCF+A, green curve), and (iii) hydrothermal synthesis with annealing only (HT+A, blue curve).

Table 1
EDX analysis results for Sample 1 after the three-step fabrication process.

Element	Apparent Conc. (wt%)	Intensity (cps)	Weight%	Weight% sigma	Atomic%
O K	3.24	0.4275	7.58	0.45	76.88
Ti K	4.28	0.8530	5.02	0.13	16.99
Sn L	3.46	0.8415	4.11	0.15	5.62
Au M	0.49	0.7778	0.62	0.17	0.51
Total	—	—	17.33	—	—

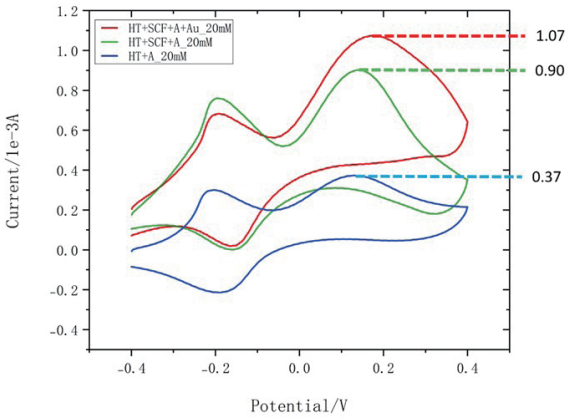

Fig. 6. (Color online) CV curves of glucose sensors in 20 mM glucose solution: HT+A (blue), HT+SCF+A (green), and HT+SCF+A+Au (red). Abbreviations: HT = Hydrothermal Synthesis, SCF = Supercritical Fluid Deposition, and A = Annealing.

The current density of the Au-modified electrode (HT+SCF+A+Au) reached ~1.07 mA, which is significantly higher than those of the SCF-only electrode (~0.90 mA) and the pristine hydrothermal electrode (~0.37 mA). These results clearly demonstrate that the three steps of the fabrication process, particularly Au deposition, greatly enhance catalytic activity toward glucose oxidation. The improvement can be attributed to the increased number of active sites, enhanced charge transfer at the electrode/electrolyte interface, and reduced electron–hole recombination. Moreover, SCF-TiO_2 coating provides additional surface roughness and stability, which further supports efficient electrochemical reactions.

3.3.2 Sensitivity analysis

Sensitivity is a key performance indicator for evaluating the effectiveness of electrochemical glucose sensors. It is defined as the rate of current change per unit concentration change, as expressed in[14–16]

$$Sensitivity = \Delta I/(A \times \Delta C), \tag{2}$$

where ΔI represents the change in current (μA or mA), A is the effective electrode area (cm^2), and ΔC is the change in glucose concentration (mM or μM).

Table 2 shows both the measured current responses at 0 and 20 mM glucose concentrations and the calculated sensitivities at 0.14 V. Upon supercritical TiO_2 deposition (HT+SCF+A), the current difference between 0 and 20 mM glucose increased from 0.2043 to 0.7267 mA, resulting in a sensitivity improvement from 10.2 to 36.3 $\mu A \cdot mM^{-1} \cdot cm^{-2}$, corresponding to an enhancement of approximately 256%. After Au nanoparticle modification, the current difference further increased to 0.8236 mA, leading to a sensitivity of 41.2 $\mu A \cdot mM^{-1} \cdot cm^{-2}$, which represents an additional improvement of approximately 13.5% compared with HT+SCF+A.

These results highlight the significance of structural optimization and surface modification. The deposition of anatase-phase TiO_2 nanoparticles via supercritical fluid deposition markedly increased the density of active sites and improved charge separation efficiency, thereby boosting glucose response. The subsequent incorporation of Au nanoparticles further enhanced

Table 2
Current response and sensitivity calculation for three fabrication processes at 0.14 V under 0 and 20 mM glucose concentrations.

Sensor	0 mM (mA)	20 mM (mA)	Sensitivity ($\mu A \cdot mM^{-1} \cdot cm^{-2}$)
HT+A	0.1668	0.3711	10.2
HT+SCF+A	0.1741	0.9008	36.3
HT+SCF+A+Au	0.2264	1.05	41.2

conductivity and introduced synergistic catalytic effects, leading to the highest overall sensitivity.

To further position the proposed sensor within recent glucose-sensing research, comparisons with previously reported glucose-sensing technologies were conducted.[17–20] Ishige *et al.* developed an enzymatic extended-gate FET glucose sensor based on ferrocenyl-modified Au electrodes for redox detection.[17] Komori *et al.* proposed a CMOS-integrated glucose sensing array using enzyme-immobilized microbeads for biochemical sensing applications.[18] Hayashi *et al.* further demonstrated a self-powered continuous glucose monitoring contact lens platform for wearable healthcare applications,[19] while Kitaike *et al.* reported an ultralow-power biofuel-cell-powered sensing circuit for biomedical monitoring systems.[20] Although those techniques have led to significant progress in system integration and portability, they often involve complex device architectures or enzyme-related stability limitations. In contrast, in the present study, we focused on a relatively simple nonenzymatic electrochemical sensing platform based on TiO_2 heterostructure engineering through hydrothermal synthesis, $scCO_2$-assisted deposition, and Au modification, which provided improved sensitivity and scalable fabrication potential.

5. Conclusions

In this study, a stepwise fabrication strategy was successfully demonstrated for the development of nonenzymatic glucose sensors. By sequentially applying the hydrothermal synthesis of rutile-phase TiO_2 nanorods, the $scCO_2$-assisted deposition of anatase TiO_2 nanoparticles, and Au nanoparticle sputtering, the sensor sensitivity progressively improved from 10.2 to 36.3 to 41.2 $\mu A \cdot mM^{-1} \cdot cm^{-2}$ at 0.14 V. Compared with the hydrothermal-only sample (HT+A), the introduction of anatase nanoparticles through supercritical deposition (HT+SCF+A) increased the sensitivity by approximately 256%, while Au modification further enhanced the performance by about 13.5%.

The enhanced sensitivity observed in the anatase/rutile heterostructure originates from the formation of homophase interfaces after annealing. When anatase and rutile phases are intimately stacked, a type-II band alignment is established, in which the conduction band minimum of rutile lies lower (by ~0.2–0.6 eV) and its valence band maximum lies higher (by ~0.7–0.8 eV) than those of anatase. This staggered alignment induces a built-in electric field that effectively drives charge carriers in opposite directions, thereby promoting the spatial separation of photogenerated electrons and holes while suppressing recombination. Consequently, more carriers successfully reach the electrode surface to participate in glucose oxidation, resulting in stronger electrochemical signals.

These findings confirm the feasibility of heterostructure engineering and surface modification for boosting the performance of TiO_2-based nonenzymatic glucose sensors. While

the full three-step modification (HT+SCF+A+Au) achieves the highest sensitivity, the two-step process (HT+SCF+A) already provides significant enhancement at a potentially lower cost, offering a practical pathway for large-scale production. Overall, the results of this study provide both experimental evidence and mechanistic insight into the role of phase interfaces and noble metal synergy, establishing a solid foundation for the future development of cost-effective, high-performance glucose sensors. The proposed TiO_2-based sensing platform also shows potential for future integration with miniaturized biochemical sensing systems such as wearable devices and lab-on-chip platforms.

Acknowledgments

We would like to express our gratitude for the financial support from the National Science and Technology Council (NSTC) of Taiwan, provided under Contracts Number NSTC 114-2221-E-218-011, NSTC 113-2622-E-218-005, and NSTC 113-2221-E-218-019. This support has been essential for the successful completion of the work presented in this paper.

References

1 V. S. Reddy, B. Agarwal, Z. Ye, C. Zhang, K. Roy, A. Chinnappan, R. J. Narayan, S. Ramakrishna, and R. Ghosh: Nanomaterials **12** (2022) 1082. https://doi.org/10.3390/nano12071082
2 J. Yang, J. Yin, and L. Xu: J. Alloys Compd. **1010** (2025) 177796. https://doi.org/10.1016/j.jallcom.2024.177796
3 P. Li, Y. Peng, J. Cai, Y. Bai, Q. Li, and H. Pang: Bioengineering **10** (2023) 733. https://doi.org/10.3390/bioengineering10060733
4 D.-W. Hwang, S. Lee, M. Seo, and T. D. Chung: Anal. Chim. Acta **1033** (2018) 1. https://doi.org/10.1016/j.aca.2018.05.051
5 K. Sabyrov, V. Adamson, and R. L. Penn: CrystEngComm **16** (2014) 1488. https://doi.org/10.1039/C3CE41820K
6 S. Zhang, B. Huang, Z. Jiang, J. Qian, J. Cao, Q. Feng, J. Zhang, and X. Li: Materials **16** (2023) 4010. https://doi.org/10.3390/ma16114010
7 M. Mancuso, S. Mottola, O. Sacco, V. Vaiano, and I. De Marco: Nanomaterials **13** (2023) 3130. https://doi.org/10.3390/nano13243130
8 S. Ye, H. Sun, J. Wu, L. Wan, Y. Ni, R. Wang, X. Ziang, and X. Deng: Polymers **14** (2022) 5513. https://doi.org/10.3390/polym14245513
9 Y. Tan, R. Shu, H. Xu, L. Song, R. Zhang, C. Ouyang, M. Xia, J. Hou, X. Zhang, Y. Yuan, and R. Zhang: J. Environ. Chem. Eng. **11** (2023) 110992. https://doi.org/10.1016/j.jece.2023.110992
10 Z. Yang, W. Xu, B. Yan, B. Wu, J. Ma, X. Wang, B. Qiao, J. Tu, H. Pei, D. Chen, and Q. Wu: ACS Omega **7** (2022) 2474. https://doi.org/10.1021/acsomega.1c06787
11 N. I. Chandrasekaran and M. Matheswaran: ACS Omega **5** (2020) 23502. https://doi.org/10.1021/acsomega.0c00417
12 D. K. Muthee and B. F. Dejene: Heliyon **7** (2021) e07269. https://doi.org/10.1016/j.heliyon.2021.e07269
13 S. Kashiwaya, C. Aymonier, J. Majimel, C. Olivier, A. Klein, W. Jaegermann, and T. Toupance: New J. Chem. **42** (2018) 18649. https://doi.org/10.1039/C8NJ04292F
14 F. Ostad Esmaeili, M. Tasviri, and N. Mohaghegh: New J. Chem. **46** (2022) 9880. https://doi.org/10.1039/D2NJ00549B
15 M. B. Lakshmipriya, T.-W. Chen, S.-M. Chen, M. Chandrasekaran, G. N. K. Ramesh Bapu, and M.-C. Yu: Int. J. Electrochem. Sci. **14** (2019) 7548. https://doi.org/10.20964/2019.08.67
16 R. P. Marin, S. Ishikawa, H. Bahruji, G. Shaw, S. A. Kondrat, P. J. Miedziak, D. J. Morgan, S. H. Taylor, J. K. Bartley, J. K. Edwards, M. Bowker, W. Ueda, and G. J. Hutchings: Appl. Catal. A Gen. **504** (2015) 62. https://doi.org/10.1016/j.apcata.2015.02.023
17 Y. Ishige, M. Shimoda, and M. Kamahori: Biosens. Bioelectron. **24** (2009) 1096. https://doi.org/10.1016/j.bios.2008.08.028
18 H. Komori, K. Niitsu, J. Tanaka, Y. Ishige, M. Kamahori, and K. Nakazato: Proc. 2014 IEEE Biomed. Circuits Syst. Conf. (IEEE, 2014) 464–467. https://doi.org/10.1109/BioCAS.2014.6981763
19 K. Hayashi, S. Arata, S. Murakami, Y. Nishio, A. Kobayashi, and K. Niitsu: IEEE Trans. Circuits Syst. II **65** (2018) 1360. https://doi.org/10.1109/TCSII.2018.2860636
20 H. Kitaike, H. Tagawa, S. Xu, R. Zhang, K. Liu, and K. Niitsu: IEEE Trans. Circuits Syst. II (2025) 1575–1579. https://doi.org/10.1109/TCSII.2025.3590168